

Site-selective measurement of coupled spin pairs in an organic semiconductor

S. L. Bayliss^{†,*},^{1,2,3} L. R. Weiss[†],² A. Mitioglu,⁴ K. Galkowski,⁵ Z. Yang,⁵ K. Yunusova,¹
A. Surrente,⁵ K. J. Thorley,⁶ J. Behrends,³ R. Bittl,³ J. E. Anthony,⁶ A. Rao,² R. H.
Friend,² P. Plochocka,⁵ P. C. M. Christianen,⁴ N. C. Greenham^{*,2} and A. D. Chepelianskii^{*1}

¹*LPS, Univ. Paris-Sud, CNRS, UMR 8502, F-91405, Orsay, France*

²*Cavendish Laboratory, J. J. Thomson Avenue, University of Cambridge, Cambridge CB3 0HE, UK*

³*Berlin Joint EPR Lab, Fachbereich Physik, Freie Universität Berlin, D-14195 Berlin, Germany*

⁴*High Field Magnet Laboratory (HFML-EMFL), Radboud University, 6525 ED Nijmegen, The Netherlands*

⁵*Laboratoire National des Champs Magnétiques Intenses,*

CNRS-UJF-UPS-INSA, 143 Avenue de Rangueil, 31400 Toulouse, France

⁶*Department of Chemistry, University of Kentucky, Lexington, KY 40506-0055, USA*

From organic electronics to biological systems, understanding the role of intermolecular interactions between spin pairs is a key challenge. Here we show how such pairs can be selectively addressed with combined spin and optical sensitivity. We demonstrate this for bound pairs of spin-triplet excitations formed by singlet fission, with direct applicability across a wide range of synthetic and biological systems. We show that the site-sensitivity of exchange coupling allows distinct triplet pairs to be resonantly addressed at different magnetic fields, tuning them between optically bright singlet ($S = 0$) and dark triplet, quintet ($S = 1, 2$) configurations: this induces narrow holes in a broad optical emission spectrum, uncovering exchange-specific luminescence. Using fields up to 60 T, we identify three distinct triplet-pair sites, with exchange couplings varying over an order of magnitude (0.3-5 meV), each with its own luminescence spectrum, coexisting in a single material. Our results reveal how site-selectivity can be achieved for organic spin pairs in a broad range of systems.

Spin pairs control the behavior of systems ranging from quantum circuits to photosynthetic reaction centers [1, 2]. In molecular materials, such pairs mediate a diverse range of processes such as light emission, charge separation and energy harvesting [3–5]. The relevant spin-pair may consist of two spin-1/2 particles, either in the form of a bound exciton or weakly coupled electron-hole pair, or spin-1 pairs, which have recently emerged as alternatives for efficient light emission and harvesting [6–9]. A key challenge in understanding and using such pairs is accessing the local molecular environments which support their generation and evolution within more complex structures, information which could ultimately lead to active control of their properties.

Here we demonstrate that the joint dependence of spin and electronic interactions on pair conformation provides a handle to separate such states and extract their discrete environments from a broader energetic landscape. We apply this technique to measure distinct triplet-pairs formed by singlet fission (Fig. 1A), a process which generates two spin $S = 1$ excitons from a photogenerated $S = 0$ singlet exciton, and is of great current interest for solar energy conversion [10–12]. We simultaneously extract the exchange energies and optical spectra of three different triplet-pair sites within the same material. Us-

ing a magnetic field, we tune different triplet pairs into excited-state avoided crossings, which we detect as spectral holes in an inhomogeneously broadened photoluminescence (PL) spectrum. This enables combined spin and optical characterization of these states: the fields required to induce avoided crossings directly measure the set of pair exchange-coupling strengths, while the spectral holes provide narrow, spin-specific optical profiles of the states. We extract multiple triplet-pair states with exchange couplings varying by an order of magnitude and decouple their distinct luminescence spectra from an otherwise inhomogeneously broadened background, reaching sub-nm spectral linewidths. Our results open up new means of determining structure-function relations of coupled spins and identify unambiguous pair signatures. This approach is directly applicable to a range of organic systems: from electron-hole pairs in next-generation light-emitting diodes to coupled excitons in light harvesters.

Selectively addressing exchange-coupled triplets

Despite their key role in light-emitters and harvesters, triplet pairs have only recently been discovered to form exchange-coupled states [13–17]. We start by outlining how such states can be selectively addressed to provide a site-specific measurement of their exchange interactions and associated optical spectra. Here we describe the specific case of singlet fission, but emphasise that the approach can be directly translated to many other molecular systems since spin conserving transitions are a general

[†]These authors contributed equally to this work.

*alexei.chepelianskii@u-psud.fr, ncg11@cam.ac.uk.

*Present address: Institute for Molecular Engineering, University of Chicago, Chicago, Illinois 60637, USA

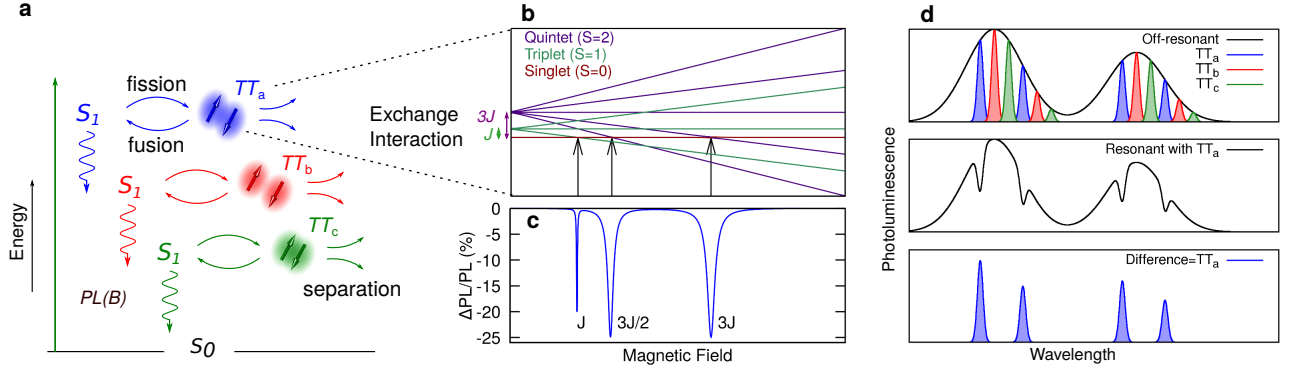


FIG. 1. Selective addressing of exchange-coupled triplet-exciton pairs. (A) Schematic of spin-pair generation by singlet fission for an ensemble of pair sites with different exchange interactions. Photon absorption generates a spin-singlet exciton (S_1), which can radiatively decay, producing photoluminescence (PL), or undergo fission into a pair of triplet excitons (TT). Fusion of this triplet pair reforms the singlet exciton, while dissociation destroys it. (B)/(C) Triplet-pair level anticrossings for a single exchange energy. A magnetic field tunes optically dark triplet or quintet spin sub-levels into near-degeneracy with the bright singlet state, resulting in selective reductions in the PL at fields proportional to the exchange interaction J . $\Delta PL/PL = [PL(B) - PL(0)]/PL(0)$. (D) The magnetic field induced anticrossings create spectral holes linked to specific triplet pair. This enables the narrow associated emission profiles of triplet pairs with different exchange interactions to be extracted.

feature of such materials.

Fig. 1A outlines the process of triplet-pair generation by singlet fission, where both fission and the subsequent fusion process are spin-conserving. This makes the spectral regions associated with triplet pairs sensitive to their spin states, which can be resonantly tuned with an external magnetic field (Fig. 1B). For strongly exchange-coupled triplets, the eigenstates at zero magnetic field consist of the pure singlet ($S = 0$), triplet ($S=1$) and quintet ($S = 2$) pairings of the two particles. Due to its singlet precursor, fission selectively populates the $S = 0$ triplet-pair configuration, which is energetically separated from the optically inactive triplet or quintet states due to the exchange interaction. Application of a magnetic field enables these triplet or quintet states to be tuned into resonance with the optically active singlet pair state when the Zeeman energy matches the singlet-triplet or singlet-quintet exchange splitting. At these field positions, bright singlet pair states become hybridized with a dark triplet or quintet pair-state, manifesting as a resonant reduction in the relevant PL spectral window (Fig. 1C) [16–18].

Crucially, the crossings directly address pairs with a specific exchange coupling. For an exchange interaction $J\mathbf{S}_1 \cdot \mathbf{S}_2$, where $\mathbf{S}_{1,2}$ are the spin operators for the two triplets, the resonances occur at $|J|$ (singlet-triplet crossing), and $3|J|/2$, $3|J|$ (singlet-quintet crossings), giving a direct measurement of the exchange. (Here we take $J > 0$ - see Supplementary Information.) Furthermore, only the emission linked to the resonant triplet pair will be diminished at each level crossing. The magnetic field resonances will therefore selectively burn spectral holes linked to pairs with a given exchange coupling (Fig. 1D). From

these resonant spectral changes, both the spin and optical properties of pair sites are therefore reconstructed. Importantly, since triplet pairs with different exchange interactions will have separated resonant fields, their associated spectra can be individually measured. Specific spin-pairs with distinct spectral and spin properties can therefore be disentangled in an ensemble measurement and their local environment and microscopic properties probed. This is the key principle of our approach to provide a spin- and site-selective measurement of coupled organic spins.

TIPS-tetracene

Of the expanding class of singlet fission materials for photovoltaic applications, solution-processable systems with a triplet energy close to the bandgap of silicon are particularly important since they could be integrated directly with established high-efficiency silicon technologies. One such material is TIPS-tetracene (Fig. 2A/B), a solution-processable derivative of the archetypal fission material tetracene [19, 20], which has been shown to undergo effective fission and generate exchange-coupled triplet pairs [13, 21, 22]. Furthermore, singlet and triplet-pair states are nearly iso-energetic in TIPS-tetracene, and so photoluminescence can be used to interrogate the fission products [21–23]. Here we use TIPS-tetracene to study the spin and electronic structure of coupled triplet excitons. To achieve both high spectral and field resolution, we perform measurements using both pulsed (< 60 T) and cw (< 33 T) magnetic fields on three identically prepared samples (Methods): Sample 1 under pulsed fields at 1.4 K, and samples 2 and 3 under cw

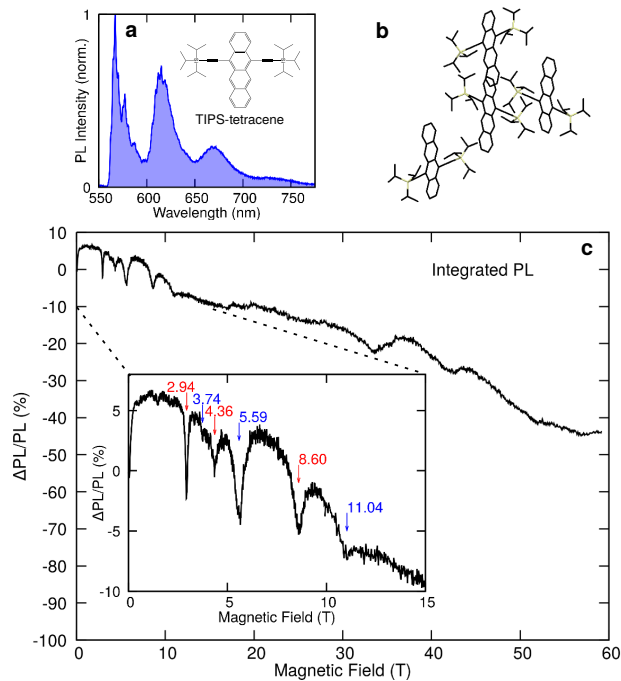


FIG. 2. Level anticrossings of spin-1 pairs. (A) Chemical schematic and photoluminescence spectrum of TIPS-tetracene at 1.4 K (Sample 1). (B) TIPS-tetracene unit cell displaying four inequivalent molecules. (C) Magneto-PL at 1.4 K integrated across all wavelengths showing a series of resonances (Sample 1, pulsed fields).

fields at 2 and 1.1 K respectively. Samples are crystallites of \sim mm linear dimensions, containing multiple domains, prepared by evaporation from saturated solution. Samples were not specifically oriented with respect to the magnetic field. We first identify triplet-pair level anticrossings in TIPS-tetracene and then use the avoided crossings to spectrally characterise multiple distinct triplet pairs.

Triplet-pair level crossings

Fig. 2C shows the changes in integrated PL up to 60 T for a TIPS-tetracene crystallite at 1.4 K (Sample 1, pulsed fields - see Methods), where $\Delta PL/PL = [PL(B) - PL(0)]/PL(0)$. Below 1 T, the conventional singlet fission magnetic-field effect is observed, indicative of weakly coupled triplet pairs [19], while at \gtrsim 1 T a very different behavior arises. On top of the monotonic PL reduction with field, which we discuss later, multiple PL resonances are apparent: a series below 15 T, and additional resonances above 30 T, indicating triplet-pair level anticrossings. As shown in Fig. 1C, for a given triplet pair there are three possible resonances with the fission-generated singlet state, occurring with field ratios 1:3/2:3. The

number of resonances in Fig. 2C therefore indicates multiple triplet pairs with different exchange interactions. While the resonances at < 15 T can be separated into two progressions with 1:3/2:3 field ratios (red/blue labels, Fig. 2C) this does not clearly assign them or associate them with particular optical properties. We now show how the identified triplet-pair level crossings can be used to unambiguously decouple and spectrally characterise multiple interacting triplets in the same material.

Spectrally resolving interacting triplets

Fig. 3B-D shows magneto-PL traces at three different wavelengths $\lambda_{a,b,c}$ which correspond to high-energy regions of the TIPS-tetracene PL spectrum (Fig. 3A). In contrast to the integrated measurements, the magneto-PL at λ_a and λ_b shows a clear progression of three resonances following the 1:3/2:3 field ratios expected for level anticrossings with the singlet state (Fig. 3C, *inset*), giving exchange interactions of 0.44 and 0.34 meV respectively, i.e. $J/g\mu_B = 3.79, 2.96$ T where $g \simeq 2$ is the exciton g -factor [13, 23] and μ_B the Bohr magneton. (Note that due to their spectral proximity, the 5.6 T λ_a resonance is also present in the λ_b trace.) In contrast to the $\lambda_{a,b}$ spectral positions, at λ_c , resonances are present only at much higher fields of 33.4 and 42.0 T. Since these do not occur at the expected 1:3/2 field ratios, we assign them to the lowest field - i.e. singlet-triplet - anticrossings of distinct triplet pairs with exchange interactions of 3.87 and 4.87 meV respectively ($J/g\mu_B = 33.4, 42.0$ T). This is further supported by their distinct temperature dependences which we describe later.

As outlined in Fig. 1D, since the PL resonances for triplet pairs with different exchange interactions are readily separable in field, we can determine their emission characteristics from the spectral components that are diminished at each resonant field position i.e., the difference in PL (ΔPL_{res}) when off-resonance vs. on resonance: $\Delta PL_{\text{res}} = |PL(B_{\text{res}}) - PL(B_{\text{off res}})|$. (We note that for an accurate off-resonance subtraction in the presence of more slowly changing non-resonant field effects, we take $PL(B_{\text{off res}})$ as the average of the spectra either side of the resonance.) The spectra associated with each set of resonances (i.e. triplet pairs) are shown in Fig. 3E-H and we label the associated triplet pairs $TT_{a,b,c}$. The resulting PL spectra show similar vibronic progressions, yet shifted peak emission energies with peaks centered at $\lambda_{a,b,c}$ (Fig. 3E). The fact that the three spectra exhibit near-identical vibrational progressions but with an overall shift relative to each other shows that the states differ predominantly in their electronic rather than vibrational coupling. The relative shift indicates a difference in the local environment between the triplet pairs which results in distinct electronic interactions with the surrounding molecules. The question arises as to why a

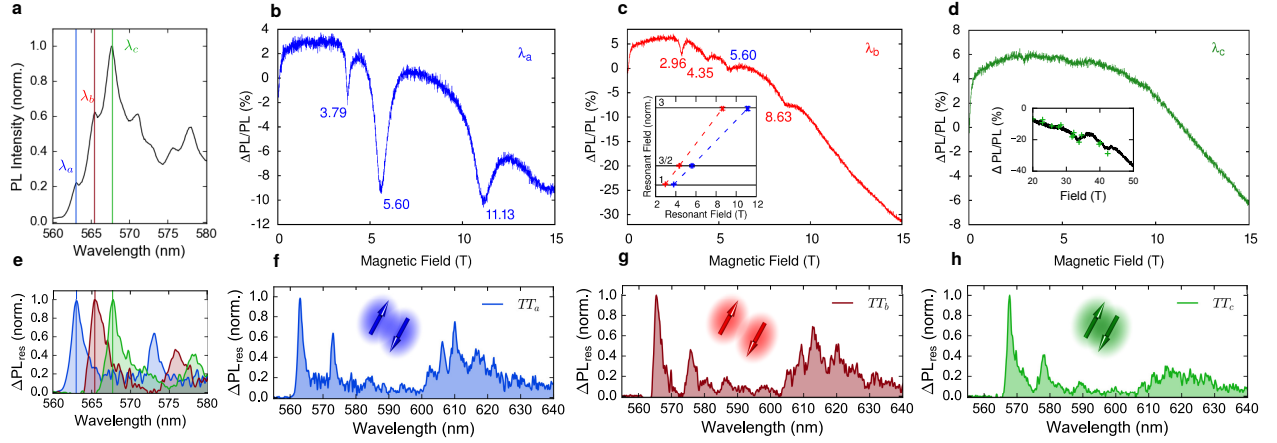


FIG. 3. Magneto-optical spectroscopy of triplet pairs formed by singlet fission. (A) 1.4 K PL spectrum with features at $\lambda_a = 562.5$ nm, $\lambda_b = 564.9$ nm, $\lambda_c = 567.1$ nm highlighted (Sample 1). (B)-(D) Magneto-PL traces for the three spectral positions λ_{a-c} (Sample 2). (B)/(C) Magnetic field resonances at λ_a and λ_b corresponding to triplet pairs with exchange interactions of 0.44 and 0.34 meV ($J/g\mu_B = 3.79, 2.96$ T). (C)-inset, resonant fields appear with ratios 1:3/2:3, as expected for the possible level crossings with the singlet state. Error bars taken as 10 % of the resonant linewidths. Dashed lines are guides to the eye. (D)-inset. Spectrally resolved PL measurements (marked field points) and integrated PL for reference (solid line) at λ_c . (E)-(H). Extracted spectra for the triplet pairs associated with the resonances (Sample 1): overlaid (E), and shown individually (F)-(H).

single material supports multiple triplet-pair sites with distinguishable electronic and spin energy levels. A natural explanation is the different molecular configurations accessible in TIPS-tetracene in which there are four rotationally inequivalent molecules in the crystal unit cell (Fig. 2B) [24]. Multiple triplet pairs may therefore be supported. Due to their differing interaction strengths and electronic environments each pair is associated with different exchange couplings and optical emission spectra. (We note that as an alternative approach to species extraction, we find that independent spectral decomposition algorithms show good agreement with the spectra/lineshapes in Fig. 3 - see Supplementary Information.)

Vibrational structure in TT spectra

In keeping with previous assignments, the first spectral peaks at $\gtrsim 560$ nm are attributed to 0-0, i.e. zero-phonon, transitions [22]. This is also consistent with the greater overlap of low-energy modes on the higher-order vibrational transitions described in detail below (Fig. 4B). Sample 3 (measured at the lowest temperature) exhibited pronounced TT_a signatures (Fig. 4A), with linewidths of the extracted spectra reaching as low as 0.5 nm (15 cm^{-1}), significantly narrower than the ~ 10 nm linewidth of the 0-0 peak in the steady-state PL spectrum. This allows us to identify the vibronic transitions shown in Fig. 3 with greater accuracy (Fig. 4B).

(Note that Sample 2 spectra - Fig. 3F-H - were measured using a spectrometer with lower spectral resolution, limiting the minimum linewidths). We use this spectrum to extract four ground-state vibrational modes involved in the emission process. Fig. 4B shows a stick spectrum of the progression of one lower energy mode with wavenumber $\nu_1 = 310 \text{ cm}^{-1}$, and three higher energy modes ($\nu_2, \nu_3, \nu_4 = 1160, 1270$, and 1370 cm^{-1}), showing good agreement with the measured spectra. These frequencies are in agreement with modes found in the ground state Raman of TIPS-Tetracene films [22] with ν_1 similar to typical C-C-C out-of plane bending modes and ν_{2-4} similar to typical C-C stretching/C-C-H bending modes [25].

To our knowledge these are the first measurements of narrow optical spectra which can be associated with triplet pairs. The sub-nm optical linewidths obtained here are comparable to those obtained in fluorescence line narrowing experiments of tetracene [26], highlighting the sensitivity of this approach. In contrast to all-optical measurements, the spin-sensitivity afforded here allows clear assignment to triplet pairs. In addition, we note that spectral extraction of triplet-pair signatures does not require clearly visible peaks in the bare PL spectrum. For example, the longer wavelength peaks associated with TT_{a-c} are unclear in the bare PL, and spectral decomposition of TT signatures is possible even in a sample with barely visible $\lambda_{a,b}$ peaks (Supplementary Information).

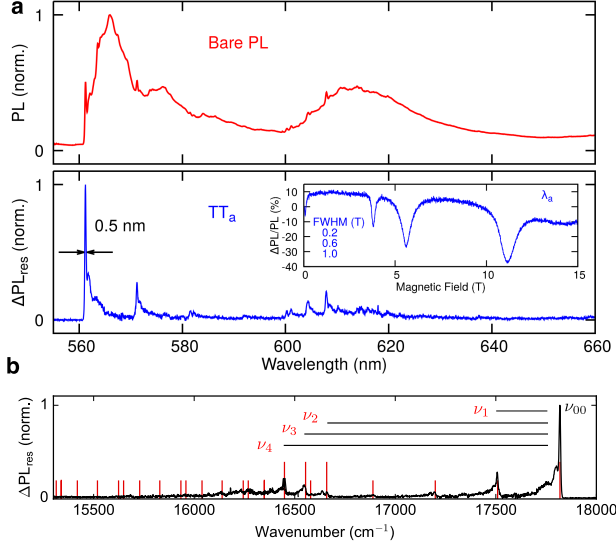


FIG. 4. Vibrational structure in sub-nm resonant PL. (A) Zero-field PL spectrum, TT_a spectrum extracted from the 5.6 T resonance and PL resonances for Sample 3. (B) Resonant PL spectrum of TT_a with idealised vibrational progression (red lines) consisting of the 0-0 transition (ν_{00}), a dominant low-energy mode with wavenumber $\nu_1 = 310 \text{ cm}^{-1}$ and three higher energy modes $\nu_2, \nu_3, \nu_4 = 1160, 1270$, and 1370 cm^{-1} .

Temperature-dependent TT signatures

The identified triplet-pair species are further distinguishable through their temperature dependences. Fig. 5A shows the temperature dependence of the resonances in the integrated PL and the corresponding evolution of the emission spectrum. By 10 K, the resonances below 15 T are lost, concurrent with the loss of the λ_a and λ_b spectral features (Fig. 5B). The fact that the resonances at ≈ 33 and 42 T have distinct temperature dependences supports their assignment to the first crossing of different triplet pairs (rather than a single species with a more structured exchange interaction [27]). By 30 K, no PL resonances are observed, with no magnetic-field effect beyond ~ 1 T. Measurement of PL spectra between 4.2-1.4 K (Fig. 5C) shows that the $\lambda_{a,b}$ spectral features evolve significantly over this temperature range, indicating that escape from the associated emission sites has an activation temperature on the order of a few Kelvin ($\sim 0.1 \text{ meV}$). Interestingly, this is approximately the exchange coupling for $TT_{a,b}$. However, we note that this energy scale may alternatively be: (i) a reorganisation energy due to molecular reconfiguration or (ii) an electronic barrier between different excited states.

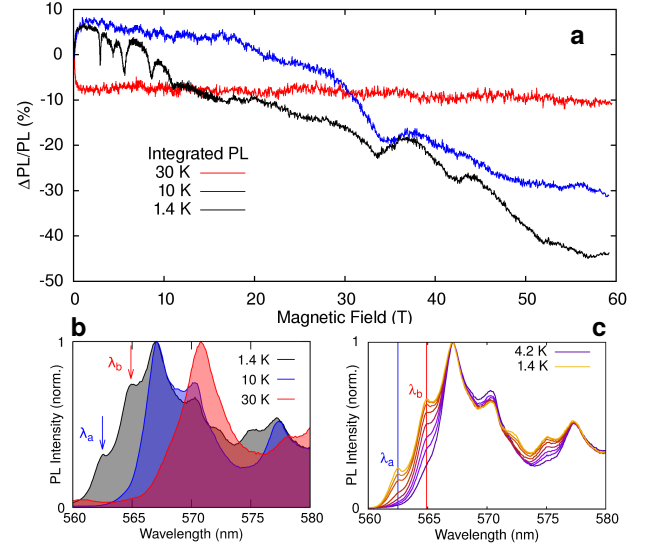


FIG. 5. Temperature dependence of triplet-pair signatures. (A)/(B) Temperature-dependent integrated PL traces and spectra (Sample 1). (C) Low-temperature behavior of the λ_a and λ_b spectral features which correspond to the triplet pairs with $J/g\mu_B = 3.79$ and 2.96 T respectively (Sample 1).

High-field spin mixing

While resonant spectral analysis provides a window into the electronic structure associated with triplet pairs, the magnetic lineshapes provide insight into spin-mixing mechanisms and the emissive species. The magneto-PL shows a monotonic decrease with field, up to nearly 50 % at 60 T (Fig. 2C), a drastically higher field than the < 0.5 T scale usually seen in organic systems. This unanticipated high-field effect can be explained due to g -factor anisotropy which can non-resonantly mix the singlet $|S\rangle$ and $m = 0$ triplet state $|T_0\rangle$, when triplets are orientationally inequivalent, analogous to Δg effects observed in spin-1/2 pairs due to differences in isotropic g -values [4, 28, 29]. The competition between spin-mixing Δg Hamiltonian terms and total-spin-conserving exchange terms sets a characteristic saturation field for the effect $\propto J/\Delta g_{\text{eff}}$, where Δg_{eff} is the relevant effective g -factor difference (Supplementary Information). Triplet pairs with a larger exchange interaction should therefore have a larger characteristic field scale for this effect and hence also be distinguishable through their non-resonant spin-mixing. Fig. 6C shows $\Delta\text{PL}/\text{PL}$ for the three different spectral regions λ_{a-c} up to 68 T. The $\lambda_{a,b}$ traces, which correspond to triplet pairs with similar exchange interactions (0.44 and 0.34 meV) show a similar non-resonant lineshape which saturates around 30 T, while the λ_c trace, associated with an order of magnitude larger exchange interaction shows a much higher characteristic field scale for PL reduction, consistent with this mechanism. We note that high-field effects have rarely

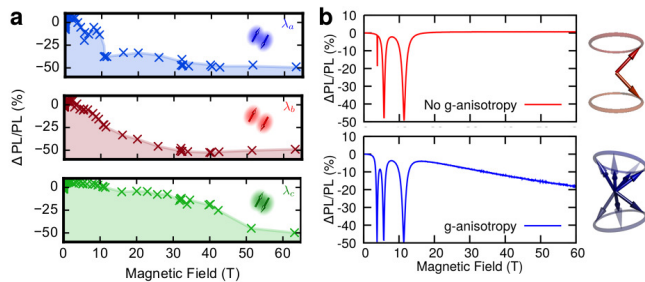


FIG. 6. Triplet-pair spin-mixing. (A) Spectrally resolved high-field effect (Sample 1) showing $\Delta PL/PL$ at spectral positions λ_{a-c} . (B) Simulation of the role of g -anisotropy. Inclusion of an anisotropic g -factor enhances the singlet-triplet level crossing (at field $J/g\mu_B = 3.8$ T) and produces a monotonic reduction in PL with field.

been observed in organic materials in general, and our observations show the relevance of spin-orbit coupling (responsible for g -anisotropy), which is usually assumed to be negligible.

Singlet-triplet level-crossings

A difference in g -matrices also provides a mixing mechanism for the singlet-triplet crossings. Since the pure $S = 1$ triplet-pair states are antisymmetric with respect to particle-exchange, while the $S = 0, 2$ states are symmetric [19], different mixing mechanisms are required for singlet-triplet vs. singlet-quintet hybridization. Singlet-quintet mixing can be mediated by the intratriplet zero-field splitting interaction [18] which characterises the dipolar interaction between electron and hole and has strength $D/g\mu_B = 50$ mT in TIPS-tetracene [13, 23, 24, 30]. However, to first order this coupling, leaves the singlet-triplet crossing forbidden (Supplementary Information). Clear singlet-triplet crossings seen for $TT_{a,b}$ therefore indicate an additional mixing mechanism. As with the high-field effect, this can be provided by a $\Delta \mathbf{g}$ Hamiltonian term which mixes singlet and triplets to first order (Fig. 6B and Supplementary Information) with strength $\sim \Delta g'_{\text{eff}} B \sim 10^{-3} B$ for an expected $\Delta g'_{\text{eff}} \sim 10^{-3}$ [31]. Additionally, this crossing can be mediated by hyperfine interactions, with typical strengths of \sim mT in organic semiconductors [32, 33].

The role of kinetics in magnetic field effect

Interestingly, the magnetic linewidths of the PL resonances (Fig. 4A) are larger than expected based purely on the mixing matrix elements for the crossings, which would give linewidths of $\lesssim 50$ mT. We obtained similar linewidths in a single crystal sample (Supplementary

Information), and therefore a distribution in J can be ruled out as the dominant line broadening mechanism. Instead, as detailed in the Supplementary Information, this indicates the resonance are predominantly broadened by the kinetics of the fission/fusion process. For both resonant and non-resonant PL reductions, mixing is predominantly between the singlet, and one other (triplet or quintet) pair state, and this sets a maximum $\Delta PL/PL$ of $\simeq 50$ % (neglecting annihilation to a single triplet). This maximum is based on the distribution of $S = 0$ character across one state at zero-field, vs. two states at resonant positions/high field [18]. The fact that the PL can be reduced by nearly 50 % by a magnetic field (Fig. 2C, Fig. 4A) therefore indicates that strongly coupled triplet pairs can dominate the steady-state emission properties of singlet-fission systems. For identifying singlet fission, the observation that exchange-coupled triplets can dominate steady-state magnetic field effects is highly significant. Often, a low-field effect ($\lesssim 100$ mT) characteristic of weakly coupled triplets [19] is taken to be a signature of the fission process [6]. In contrast, our results show that singlet fission magnetic field effects can be drastically different between strongly and weakly coupled triplets, and that high-field effects ($\gtrsim 1$ T) can instead dominate.

We note that for fission generated triplet pairs the emissive species may either be a distinct singlet exciton or, as proposed recently [22, 34], the triplet pairs themselves. While typically challenging to distinguish these scenarios, the combination of kinetically broadened linewidths and near 50 % resonant PL reductions naturally arises only when triplet pairs emit via a separate singlet state, rather than directly themselves, showing the additional utility of these measurements in distinguishing these kinetic scenarios (Supplementary Information).

Outlook

The magneto-optic resolution of organic triplet pairs opens up the possibility to correlate their exchange and electronic structure with their chemical environment and physical conformation. Since the mixing matrix elements relevant for the PL resonances depend on the relative orientation between the external field and the triplet pair [18], measuring orientationally dependent PL resonances should allow triplet pairs to be assigned to specific molecular configurations. Identification of unambiguous spectral signatures of triplet pairs further means that these states can now be studied through purely optical means. For example, triplet-pair microscopy could be used to obtain information on the spatial distribution of pair sites across microcrystalline domains and map their diffusion [35–37], and resonant excitation could be used to address specific triplet pairs through site-specific fluorescence [38, 39].

While here we spectrally resolve triplet pairs in a sin-

glet fission material, these results are applicable to a range of other organic spin-pair systems. For example, triplet-triplet encounters are pivotal in photovoltaic up-conversion systems [40] and organic light-emitting diodes [9, 41], and triplet-pair level anticrossings should also be observable in photovoltaic device architectures, where resonances could be measured through solar-cell photocurrent or quantum-dot emission [11]. In spin-1/2 pairs, analogous spectrally resolved level crossings should help to clarify the spin and electronic structure of the emissive species central to thermally activated delayed fluorescence in next-generation organic light-emitting diode materials, and extracting optical signatures from level-crossings observed in synthetic and biological radical pairs should provide further insights into these key intermediates [4, 33, 42, 43]. Finally, the nanoscale sensitivity of exchange-coupled spins opens up the possibility to deliberately engineer them as joint spin-optical probes of complex molecular systems.

-
- [1] Petta, J. R. *et al.* Coherent manipulation of coupled electron spins in semiconductor quantum dots. *Science* **309**, 2180–2184 (2005).
 - [2] Lubitz, W., Lendzian, F. & Bittl, R. Radicals, radical pairs and triplet states in photosynthesis. *Acc. Chem. Res.* **35**, 313–320 (2002).
 - [3] Clarke, T. M. & Durrant, J. R. Charge photogeneration in organic solar cells. *Chem. Rev.* **110**, 6736–67 (2010).
 - [4] Steiner, U. & Ulrich, T. Magnetic field effects in chemical kinetics and related phenomena. *Chem. Rev.* **89**, 51–147 (1989).
 - [5] McCamey, D. *et al.* Spin rabi flopping in the photocurrent of a polymer light-emitting diode. *Nat. Mat.* **7**, 723 (2008).
 - [6] Congreve, D. N. *et al.* External quantum efficiency above 100% in a singlet-exciton-fission-based organic photovoltaic cell. *Science* **340**, 334–7 (2013).
 - [7] Mezyk, J., Tubino, R., Monguzzi, A., Mech, A. & Meinardi, F. Effect of an external magnetic field on the up-conversion photoluminescence of organic films: The role of disorder in triplet-triplet annihilation. *Phys. Rev. Lett.* **102**, 087404 (2009).
 - [8] Liu, R., Zhang, Y., Lei, Y., Chen, P. & Xiong, Z. Magnetic field dependent triplet-triplet annihilation in alq3-based organic light emitting diodes at different temperatures. *J. Appl. Phys.* **105**, 093719 (2009).
 - [9] van Eersel, H., Bobbert, P. & Coehoorn, R. Kinetic monte carlo study of triplet-triplet annihilation in organic phosphorescent emitters. *J. Appl. Phys.* **117**, 115502 (2015).
 - [10] Smith, M. B. & Michl, J. Singlet fission. *Chem. Rev.* **110**, 6891–936 (2010).
 - [11] Thompson, N. J. *et al.* Energy harvesting of non-emissive triplet excitons in tetracene by emissive PbS nanocrystals. *Nat. Mater.* **13**, 1039–1043 (2014).
 - [12] Tabachnyk, M. *et al.* Resonant energy transfer of triplet excitons from pentacene to PbSe nanocrystals. *Nat. Mater.* **13**, 1033–1038 (2014).
 - [13] Weiss, L. R. *et al.* Strongly exchange-coupled triplet pairs in an organic semiconductor. *Nat. Phys.* **13**, 176–181 (2017).
 - [14] Tayebjee, M. J. *et al.* Quintet multiexciton dynamics in singlet fission. *Nat. Phys.* **13**, 182–188 (2017).
 - [15] Basel, B. S. *et al.* Unified model for singlet fission within a non-conjugated covalent pentacene dimer. *Nat. Commun.* **8**, 15171 (2017).
 - [16] Wakasa, M. *et al.* What can be learned from magnetic field effects on singlet fission: role of exchange interaction in excited triplet pairs. *J. Phys. Chem. C* **119**, 25840–25844 (2015).
 - [17] Yago, T., Ishikawa, K., Katoh, R. & Wakasa, M. Magnetic field effects on triplet pair generated by singlet fission in an organic crystal: Application of radical pair model to triplet pair. *J. Phys. Chem. C* **120**, 27858–27870 (2016).
 - [18] Bayliss, S. L. *et al.* Spin signatures of exchange-coupled triplet pairs formed by singlet fission. *Phys. Rev. B* **94**, 045204 (2016).
 - [19] Merrifield, R. E. Magnetic effects on triplet exciton interactions. *Pure Appl. Chem.* **27**, 481–498 (1971).
 - [20] Burdett, J. J., Piland, G. B. & Bardeen, C. J. Magnetic field effects and the role of spin states in singlet fission. *Chem. Phys. Lett.* **585**, 1–10 (2013).
 - [21] Stern, H. L. *et al.* Identification of a triplet pair intermediate in singlet exciton fission in solution. *Proc. Nat. Acad. Sci.* **112**, 7656–7661 (2015).
 - [22] Stern, H. L. *et al.* Ultrafast triplet pair formation and subsequent thermally activated dissociation control efficient endothermic singlet exciton fission. *Nat. Chem.* (2017).
 - [23] Bayliss, S. L. *et al.* Geminate and Nongeminate Recombination of Triplet Excitons Formed by Singlet Fission. *Phys. Rev. Lett.* **112**, 238701 (2014).
 - [24] Bayliss, S. L. *et al.* Localization length scales of triplet excitons in singlet fission materials. *Phys. Rev. B* **92**, 115432 (2015).
 - [25] Alajtal, A., Edwards, H., Elbagerma, M. & Scowen, I. The effect of laser wavelength on the raman spectra of phenanthrene, chrysene, and tetracene: Implications for extra-terrestrial detection of polyaromatic hydrocarbons. *Spectrochim. Acta Mol. Spectrosc.* **76**, 1–5 (2010).
 - [26] Hofstra, J., Schenkeveld, A., Engelsma, M., Gooijer, C. & Velthorst, N. Temperature effects on fluorescence line narrowing spectra of tetracene in amorphous solid solutions. analytical implications. *Spectrochim. Acta Mol. Spectrosc.* **45**, 139–146 (1989).
 - [27] Kollmar, C., Sixl, H., Benk, H., Denner, V. & Mahler, G. Theory of two coupled triplet states-electrostatic energy splittings. *Chem. Phys. Lett.* **87**, 266–270 (1982).
 - [28] Devir-Wolfman, A. H. *et al.* Short-lived charge-transfer excitons in organic photovoltaic cells studied by high-field magneto-photocurrent. *Nat. Commun.* **5** (2014).
 - [29] Wang, Y., Sahin-Tiras, K., Harmon, N. J., Wohlgenannt, M. & Flatté, M. E. Immense magnetic response of exciplex light emission due to correlated spin-charge dynamics. *Phys. Rev. X* **6**, 011011 (2016).
 - [30] Weil, J. A. & Bolton, J. R. *Electron Paramagnetic Resonance*, chap. 6, 162–187 (Wiley, New Jersey, 2007).
 - [31] Schott, S. *et al.* Tuning the effective spin-orbit coupling in molecular semiconductors. *Nat. Commun.* **8** (2017).
 - [32] McCamey, D. *et al.* Hyperfine-field-mediated spin beating in electrostatically bound charge carrier pairs. *Phys. Rev. Lett.* **104**, 017601 (2010).
 - [33] Zarea, M., Carmieli, R., Ratner, M. A. & Wasielewski, M. R. Spin dynamics of radical pairs with restricted ge-

- ometries and strong exchange coupling: The role of hyperfine coupling. *J. Phys. Chem. A* **118**, 4249–4255 (2014).
- [34] Yong, C. K. *et al.* The entangled triplet pair state in acene and heteroacene materials. *Nat. Commun.* **8** (2017).
- [35] Irkhin, P. & Biaggio, I. Direct imaging of anisotropic exciton diffusion and triplet diffusion length in rubrene single crystals. *Phys. Rev. Lett.* **107**, 017402 (2011).
- [36] Akselrod, G. M. *et al.* Visualization of exciton transport in ordered and disordered molecular solids. *Nat. Commun.* **5**, 3646 (2014).
- [37] Wan, Y. *et al.* Cooperative singlet and triplet exciton transport in tetracene crystals visualized by ultrafast microscopy. *Nat. Chem.* **7**, 785 (2015).
- [38] Bässler, H. & Schweitzer, B. Site-selective fluorescence spectroscopy of conjugated polymers and oligomers. *Acc. Chem. Res.* **32**, 173–182 (1999).
- [39] Orrit, M., Bernard, J. & Personov, R. High-resolution spectroscopy of organic molecules in solids: from fluorescence line narrowing and hole burning to single molecule spectroscopy. *J. Phys. Chem.* **97**, 10256–10268 (1993).
- [40] Singh-Rachford, T. N. & Castellano, F. N. Photon up-conversion based on sensitized triplet-triplet annihilation. *Coord. Chem. Rev.* **254**, 2560–2573 (2010).
- [41] Baldo, M. A., Adachi, C. & Forrest, S. R. Transient analysis of organic electrophosphorescence. ii. transient analysis of triplet-triplet annihilation. *Phys. Rev. B* **62**, 10967 (2000).
- [42] Weiss, E. A., Ratner, M. A. & Wasielewski, M. R. Direct measurement of singlet- triplet splitting within rod-like photogenerated radical ion pairs using magnetic field effects: Estimation of the electronic coupling for charge recombination. *J. Phys. Chem. A* **107**, 3639–3647 (2003).
- [43] Hiscock, H. G. *et al.* The quantum needle of the avian magnetic compass. *Proc. Nat. Acad. Sci.* **113**, 4634–4639 (2016).
- [44] Eaton, D. *et al.* CCDC 962667: Experimental Crystal Structure Determination, DOI: 10.5517/cc119qsv. (2014).

Methods

Samples were excited by 532, 514 or 485 nm laser illumination (similar results were obtained across this wavelength range). A long-pass filter was used to remove the laser line, and the collected PL was either sent to an avalanche photodiode for the integrated measurements or through a monochromator to a nitrogen-cooled CCD for the spectrally resolved measurements. Three different TIPS-tetracene crystallites prepared by evaporation from saturated solution were used which we refer to as samples 1-3. X-Ray diffraction confirmed that all samples indexed to the same unit cell previously determined for TIPS-tetracene [44], demonstrating that they had the same underlying solid-state structure. Integrated and spectrally resolved experiments to 68 T were performed using Sample 1 under pulsed magnetic field at LNCMI Toulouse. Spectrally resolved measurements up to 33 T were performed using samples 2 and 3 under steady-state fields at the HFML, Nijmegen. For low-temperature measurements samples were either immersed in liquid helium (Samples 1 and 3) or cooled via exchange gas with a surrounding helium bath (Sample 2), giving base temperatures of $\simeq 1.4$, 2 and 1.1 K for

samples 1-3 respectively. PL spectra in Fig. 5C were taken with Sample 1 in helium under continuous pumping. Further details and comparison of the samples are contained in the Supplementary Information.

Acknowledgements

This work was supported by HFML-RU/FOM and LNCMI-CNRS, members of the European Magnetic Field Laboratory (EMFL) and by EPSRC (UK) via its membership to the EMFL (grant no. EP/N01085X/1 and NS/A000060/1) and through grant no. EP/M005143/1. L.R.W. acknowledges support of the Gates-Cambridge and Winton Scholarships. We acknowledge support from Labex ANR-10-LABX-0039-PALM, and ANR SPINEX. We are grateful for support from DFG SPP-1601 (Bi-464/10-2).

Author contributions

S.L.B. and L.R.W. analysed the data and wrote the manuscript with input from all authors. S.L.B., L.R.W., A.M. and K.Y. carried out the experiments at the HFML. S.L.B., L.R.W., K.G., Z.Y., K.Y., A.S. and A.D.C. carried out the experiments at the LNCMI. K.J.T. and J.E.A. provided the materials. All authors discussed the results.

Additional information

Correspondence should be addressed to A.D.C or N.C.G., and requests for materials to J.E.A (anthony@uky.edu).

Competing financial interests

The authors declare no competing financial interests.

Supplementary Information: Site-selective measurement of coupled spin pairs in an organic semiconductor

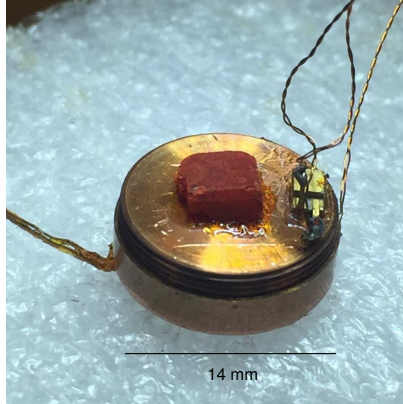


FIG. S1. TIPS-tetracene crystallites. Photograph of Sample 3 mounted on sample holder.

I. SAMPLES

Samples were prepared by evaporation from saturated solution. In the main text, three samples were used which we refer to as samples 1-3. These samples were crystallites of \sim mm linear dimensions, containing multiple domains (each of $100\text{ }\mu\text{m}$ scale) with a powder coating. Fig. S1 shows an image of Sample 3, Samples 1 and 2 were prepared in an identical way. X-Ray diffraction confirmed that all samples indexed to the same unit cell previously determined for TIPS-tetracene, demonstrating that they had the same underlying solid-state structure.

In addition, a separate single crystal sample, which showed good extinction under crossed-polarizers, was used to investigate the origin of the broadening of the photoluminescence resonances. These data are described in Section V below.

II. PL AND $\Delta\text{PL}_{\text{res}}$ SPECTRA IN SAMPLES 1-3

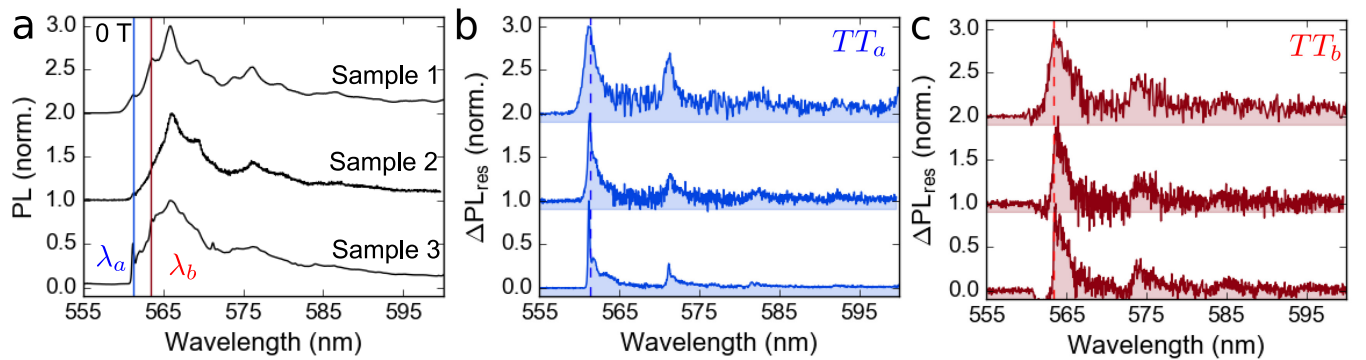


FIG. S2. Photoluminescence and triplet-pair site emission for samples 1-3. **a** Zero-field emission with spectral positions $\lambda_{a,b}$ highlighted. **b** Extracted TT_a spectra using the 5.6 T resonance for samples 1-3 (top to bottom). **c** Extracted TT_b spectra taken using the 2.98 T resonance for samples 1-3 (top to bottom).

Three samples, labelled 1-3, were used, as described in the main text. Each sample was measured under slightly different conditions: Sample 1 and 3 were measured at 1.4 K and 1.1 K respectively, both immersed in liquid helium, while Sample 2 was measured at 2 K under exchange gas. Fig. S2 shows that the relative intensities of TT_{a-c} in the

bare PL vary between samples, as well as their extracted linewidths, but not the peak positions/vibronic structure. We note that the grating used for Sample 2 and 3 afforded higher spectral resolution than that used for Sample 1, which contributes to differences in the observed linewidths.

III. EXTRACTION OF $\Delta\text{PL}_{\text{res}}$

As described in the main text, resonant spectra were extracted by taking the difference in PL on and off resonance:

$$\Delta\text{PL}_{\text{res}} = |\text{PL}(B_{\text{res.}}) - \text{PL}(B_{\text{off res.}})|. \quad (\text{S1})$$

Here we describe this procedure in detail for both cw and pulsed magnetic fields.

A. Resonant Spectra from Continuous Magnetic Field Sweeps

For Sample 2 and 3, the magnetic field was continuously swept and spectra continuously recorded. For a clean off-resonant subtraction, $\text{PL}(B_{\text{off res.}})$ was taken as the average of spectra at symmetric points either side of each resonance:

$$\Delta\text{PL}_{\text{res}} = |\text{PL}(B_{\text{res.}}) - \text{PL}(B_{\text{off res.}})| = |\text{PL}(B_0) - \frac{1}{2}[\text{PL}(B_0 + \Delta) + \text{PL}(B_0 - \Delta)]|, \quad (\text{S2})$$

where B_0 is the resonant field, and Δ the field separation between the on-resonant and off-resonant points. To improve the signal-to-noise ratio, the on-resonant and off-resonant spectra were averaged within a smaller window δ .

The spectra associated with $TT_{a,b}$ for each resonant field are shown in Fig. S3. These show that the same spectra can be extracted for each field in a given resonance progression (3.79, 5.60, and 11.13 T for TT_a and 2.96, 4.35, and 8.65 T for TT_b). The parameters used to extract each spectrum are listed in Table S1. Note that resonances that overlapped with neighbouring resonances, such as the 4.25 T and 8.63 T dips, required smaller windows for off-resonant spectra (smaller Δ) and smaller averaging windows (δ).

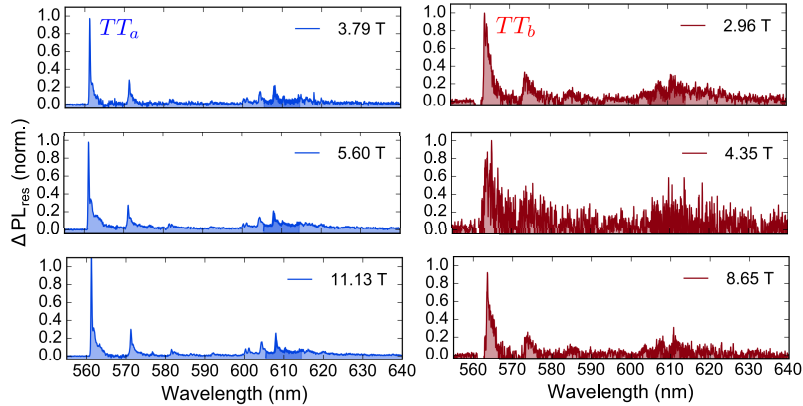


FIG. S3. $\Delta\text{PL}_{\text{res}}$ from continuous field measurements taken on Sample 3 at 1.1 K. Parameters used to extract spectra are detailed in Table 1.

B. Resonant Spectra from Pulsed Magnetic Field Points

For measurements in pulsed magnetic fields (Sample 1), fields were swept over ~ 100 ms and so spectra could only be sampled at discrete points (Fig S4g). In this case, symmetric points about the resonances were not available for off-resonant subtraction. To extract $\Delta\text{PL}_{\text{res}}$, the off-resonant spectra were therefore calculated via linear interpolation between the available field points (B_{\pm}) either side of the resonance at B_0 :

Sample 3		
B_0 (T)	Δ (T)	δ (T)
3.79	0.5	0.13
5.60	1.0	0.13
11.13	2.0	0.15
2.96	0.6	0.13
4.35	0.25	0.09
8.63	0.9	0.15

Table S1. Field positions and parameters used for $\Delta\text{PL}_{\text{res}}$ extraction for Sample 3. B_0 is the resonant field, Δ is the field step on either side of B_0 at which non-resonant spectra are taken, and δ is the averaging window used for on and off-resonant spectral slices.

$$\Delta\text{PL}_{\text{res}} = |\text{PL}(B_{\text{res.}}) - \text{PL}(B_{\text{off res.}})| = \left| \text{PL}(B_0) - \frac{\Delta_+ \text{PL}(B_+) + \Delta_- \text{PL}(B_-)}{(\Delta_+ + \Delta_-)} \right| \quad (\text{S3})$$

$$\Delta_+ = B_+ - B_0 \quad (\text{S4})$$

$$\Delta_- = B_0 - B_- \quad (\text{S5})$$

Parameters used are in Table S2. We found good agreement with spectra extracted from both cw and pulsed field measurements.

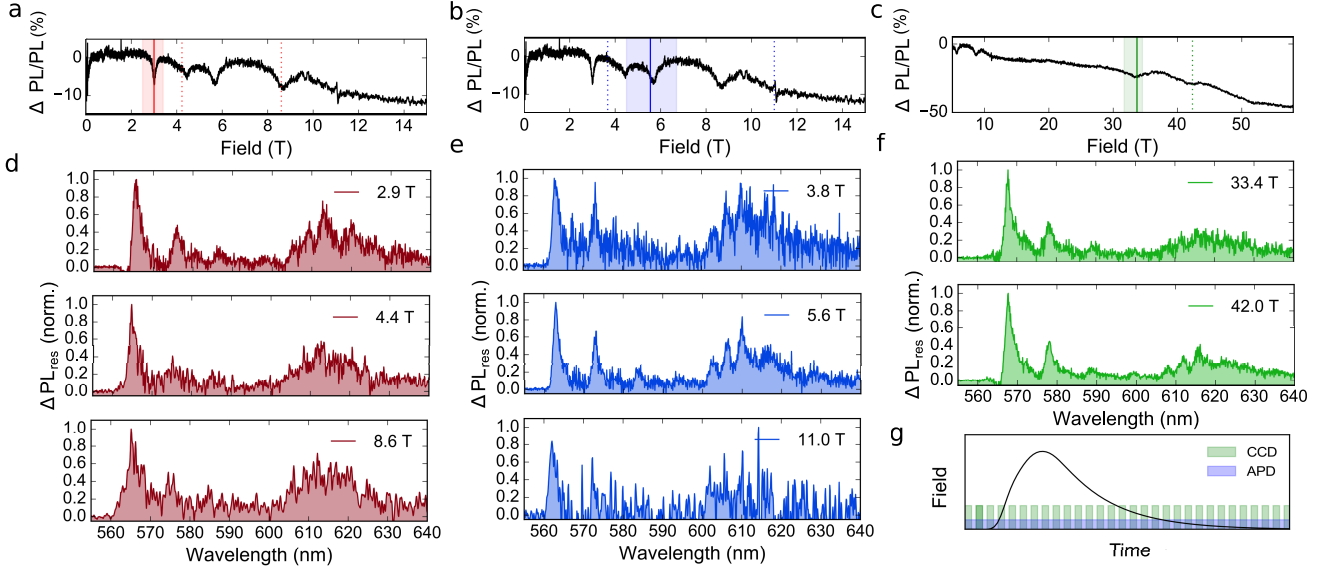


FIG. S4. $\Delta\text{PL}_{\text{res}}$ from pulsed field measurements taken on Sample 1 at 1.4 K. **a** Field points used for TT_b resonances: field point used in main text (2.9 T, solid line) and remaining resonances at 4.4 T and 8.6 T (dashed lines). **b** Field points used for TT_a resonances: field point used in main text (5.6 T, solid line) and remaining resonances at 3.8 T and 11.0 T (dashed lines). **c** Field points used for TT_c spectrum: field point used in main text (33.7 T, solid line) and remaining resonance at 42 T (dashed line). We note that while the 33 and 43 T resonances have very similar spectral features, they have distinct temperature dependences and so are associated with distinct species. **d** $\Delta\text{PL}_{\text{res}}$ for all three TT_a resonances: 2.9, 4.4, and 8.6 T. **e** $\Delta\text{PL}_{\text{res}}$ for all three TT_b resonances: 3.8, 5.6, and 11.0 T. **f** $\Delta\text{PL}_{\text{res}}$ for the high-field resonances at 33.4 T and 42.0 T. **g** Schematic of spectrally resolved PL measurements through pulsed field shots. The black line represent the field through time, the blue gate shows the continuous integrated measurement of the PL recorded on an avalanche photodiode (APD) and the green gates show the shutter (2 ms) for CCD exposure for spectrally resolved data. A series of shots to different field points were used to extract $\Delta\text{PL}_{\text{res}}$.

Resonance (T)	B_0 (T)	B_+ (T)	B_- (T)	Δ_+, Δ_- (T)
2.98	3.049	3.362	2.488	0.313, 0.561
3.79	3.673	4.235	2.488	0.562, 1.185
5.60	5.501	6.753	4.466	1.252, 1.035
4.36	4.23	6.406	2.22	2.176, 2.01
8.63	8.614	9.398	7.82	0.784, 0.794
11.13	11.67	14.66	9.292	2.99, 2.378
33.4	33.78	34.55	31.7	0.77, 2.08
42.0	42.33	-	39.77	2.56

Table S2. Field positions used for ΔPL_{res} extraction for Sample 1. Spectra in Fig. 3 of the main text used the resonances at 5.6, 2.98 and 32.4 T. Since it was not possible to extract a spectral slice at B_+ for the 43.0 T resonance, only a spectrum at B_- was used for off-resonant subtraction.

IV. NUMERICAL SPECTRAL DECOMPOSITION

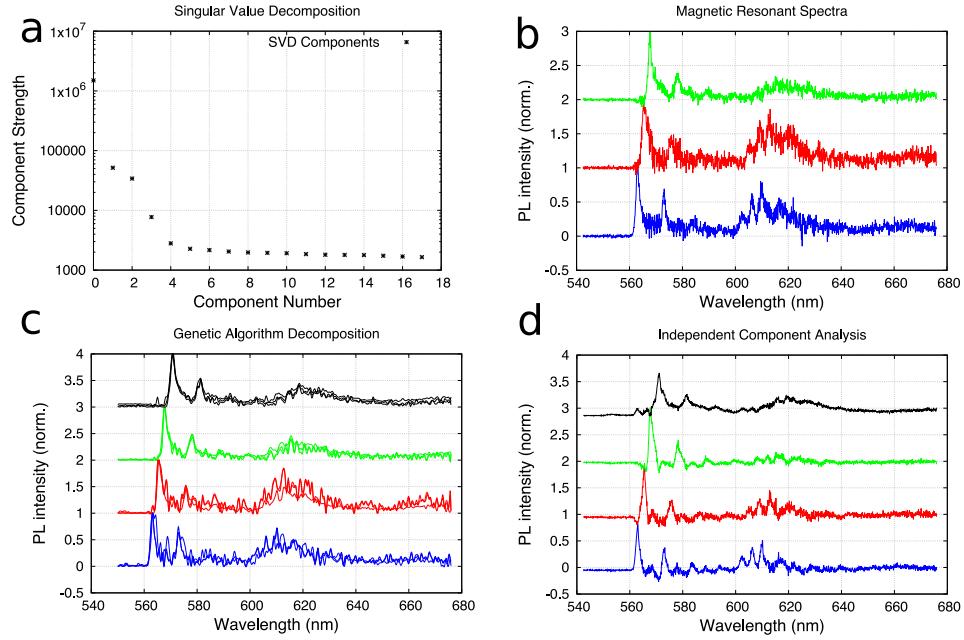


FIG. S5. Spectral decomposition of magneto-photoluminescence in Sample 2. **a** Singular value decomposition (SVD) of the field-dependent spectra for pulsed field data up to 68 T, showing four significant components. **b** Three species corresponding to distinct exchange couplings (and hence level crossings) decomposed using the magnetic level-crossing technique outlined above. **c** Spectral deconvolution into four distinct components using a genetic algorithm. **d** Spectral decomposition into four distinct components using an independent component analysis algorithm.

To complement the approach used in the main text, and provide an alternative means to extract triplet-pair optical signatures, the magnetic-field dependent photoluminescence spectrum was decomposed into separate components with machine-learning algorithms (Fig. S5). We use two distinct algorithms which both reproduce the species observed in the magnetic level-crossing technique. Using singular value decomposition, four main components are present in the spectrum above the noise (Fig. S5a). The spectra associated with those four components is then confirmed using a genetic algorithm (documented previously [S1]), shown in Fig. S5c, and separately using blind source separation using an implementation of independent component analysis in the python module “Scikit-learn” (Fig. S5c) [S2]. The results confirm the spectral separation into three distinct magnetically active components (corresponding to TT_{a-c}), with the remainder of the spectrum showing no distinct dependence on magnetic field.

V. MAGNETO-PL OF TIPS-TETRACENE SINGLE CRYSTAL

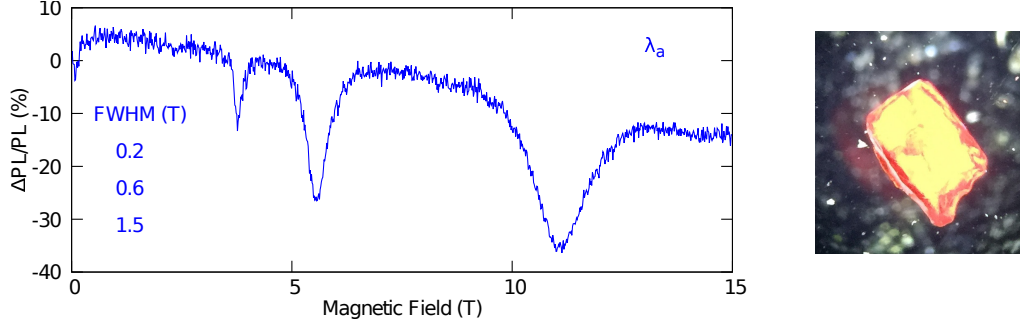


FIG. S6. Left: $\Delta\text{PL}/\text{PL}$ for a TIPS-tetracene single crystal at 1.1 K at the λ_a spectral position. Excitation was at 488 nm and the orientation of the crystal axes relative to the magnetic field was not determined. Right: crossed polarizer image of single-crystal sample highlighting its optical uniformity across the sample.

Fig. S6 shows $\Delta\text{PL}/\text{PL}$ at λ_a in a single crystal TIPS-tetracene sample (confirmed using cross-polarized optical microscopy - Fig. S6, right), displaying comparable magnetic linewidths to the multi-domain samples 1-3. This indicates that the linewidths of the PL resonances are kinetically broadened, instead of inhomogeneously broadened due to variations in exchange coupling. This kinetic broadening is described in more detail below.

VI. SPIN HAMILTONIAN AND SIGN OF J

We adopt a triplet-pair spin Hamiltonian consisting of exchange, Zeeman and zero-field splitting terms:

$$H = J\mathbf{S}_1 \cdot \mathbf{S}_2 + \sum_{i=1,2} (\mu_B \mathbf{B} \cdot \mathbf{g}_i \cdot \mathbf{S}_i + \mathbf{S}_i \cdot \mathbf{D}_i \cdot \mathbf{S}_i) \quad (\text{S6})$$

where $\mathbf{g}_{1,2}$ and $\mathbf{D}_{1,2}$ are the g - and zero-field-splitting matrices for triplets 1 and 2. For the two triplets, we assume that \mathbf{g} and \mathbf{D} differ only in their orientations and not their principal values. Resonances occur between the spin $S = 0$ triplet-pair state $|S\rangle$ and one other ($S = 2$ or $S = 1$) state $|X\rangle$, forming an effective two-level system with eigenstates $|1\rangle, |2\rangle$. The emission probability for each state depends on their singlet projections $|\langle 1|S\rangle|^2 = \frac{1}{2}[1 + (4V^2/\Delta^2 + 1)^{-1/2}]$, $|\langle 2|S\rangle|^2 = 1 - |\langle 1|S\rangle|^2$, where $V = |\langle X|H|S\rangle|$ is the mixing matrix element, $\Delta = \langle S|H|S\rangle - \langle X|H|X\rangle \simeq \frac{J}{2}S(S+1) - mg\mu_B B$ is the detuning with m the spin projection along the field. This gives resonant fields of $(1, 1.5, 3)|J|/g\mu_B$, independent of the sign of J , and so here we choose $J > 0$. Corrections to the resonant field positions of order D [S3], the triplet zero-field splitting parameter, could in principle be used to extract the sign of J with the sign of D (> 0) known for TIPS-tetracene [S4]. The linewidths of the PL resonances currently make it challenging to extract any deviations from the expected 1:1.5:3 field ratios, and so we leave this sign determination for future work.

VII. SPIN MIXINGS

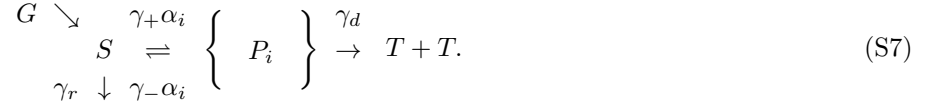
Taking colinear $\mathbf{g}_{1,2}$, we find $|\langle T_i|H|S\rangle| = 0$ making singlet-triplet mixings nominally forbidden for rotationally equivalent triplets. For orientationally inequivalent triplets, high-field spin-mixing becomes allowed with g -anisotropy through $|S\rangle - |T_0\rangle$ mixing. Taking $\mathbf{B} \parallel z$ we find $|\langle T_0|H|S\rangle|/\Delta = \sqrt{\frac{2}{3}}\mu_B B|\Delta g_{zz}|/J$, setting a characteristic saturation field $\sim J/|\Delta g_{zz}|$ where $\Delta g_{ij} = g_{1,ij} - g_{2,ij}$. The singlet-triplet resonance also becomes allowed through this mechanism, $|\langle T_-|H|S\rangle| = \frac{1}{\sqrt{3}}\mu_B B\sqrt{\Delta g_{zx}^2 + \Delta g_{zy}^2}$. Additionally, hyperfine interactions can mix singlet and triplet manifolds. Since these have strength $\sim \text{mT}$, independent of the field, they would not give rise to a high-field effect.

VIII. KINETIC MODELLING

Simulations are as described in Ref. [S3] which uses the kinetic scheme outlined in Fig. 1A, but incorporating an anisotropic triplet g -matrix. Fig. 6B uses the TIPS-tetracene zero-field splitting parameter $D/g\mu_B = 50$ mT [S4–S6], a kinetic ratio (singlet reformation rate/dissociation rate) $\epsilon = 10^3$ [S3], and a molecular g -matrix of $\mathbf{g}_{mol} = g \cdot \text{diag}(1 - \delta, 1, 1 + \delta)$ where $\delta = 0$ or 2.5×10^{-3} . Simulations are for triplets randomly oriented with respect to each other and the field. As outlined above, mixing should only be effective for $V \sim \Delta$ giving linewidths $\lesssim D$ for resonant fields $\lesssim 50$ T. For large ϵ however, the resonant linewidths are increased as $\sim \sqrt{\epsilon}$, providing an additional kinetic broadening. While the two emission scenarios (from a separate singlet and from triplet pairs directly) exhibit this kinetic broadening, in the case of triplet-pair emission, $\Delta\text{PL}/\text{PL}$ reduces as ϵ^{-1} while for separate singlet emission it saturates at 50 %, indicating the presence of triplet-pairs coupled to a site-specific emissive singlet. This is described in more detail below.

A. Singlet-Exciton Emission

As described previously [S3, S7], we adopt the following kinetic scheme for magneto-photoluminescence



Here G is the generation rate of singlet excitons (S) and γ_r their radiative decay rate. γ_{\pm} are the rates of generation and fusion of triplet-pair state P_i and $\alpha_i = \langle P_i | P_S | P_i \rangle$ is their singlet content where $P_S = |S\rangle\langle S|$ and $|S\rangle$ is the spin-singlet state. When the effective fission rate is fast compared to the radiative decay rate (i.e. fission is efficient), the steady-state photoluminescence is

$$\text{PL}(B) \simeq \frac{G\gamma_r}{\gamma_+} \left(\sum_i \frac{\alpha_i(B)}{1 + \epsilon\alpha_i(B)} \right)^{-1} \quad (S8)$$

where $\epsilon = \gamma_-/\gamma_d$. For exchange-coupled triplets at zero-field, $\alpha_i = 1$ for the singlet state and is zero for all the other states. At the level crossings, effective two-level systems are formed between the singlet state $|S\rangle$ and one other ($S = 2$ or $S = 1$) state $|X\rangle$. This gives $\{\alpha_i\} = \alpha_1, 1 - \alpha_1$ with

$$\alpha_1 = \frac{1}{2} \left(1 + \frac{1}{\sqrt{1 + 4V^2/\Delta^2}} \right), \quad (S9)$$

where $V = |\langle X | H | S \rangle|$ is the mixing matrix element from the spin-Hamiltonian H and, $\Delta = \langle S | H | S \rangle - \langle X | H | X \rangle \simeq \frac{J}{2}S(S+1) - mg\mu_B B$ is the detuning with m the spin projection along the field. This yields

$$\frac{\Delta\text{PL}}{\text{PL}} = -\frac{\epsilon}{2(\epsilon+1)} \frac{1}{1 + \left(\frac{\Delta}{V\sqrt{2(\epsilon+2)}} \right)^2}. \quad (S10)$$

At resonance, $\Delta = 0$ giving

$$\frac{\Delta\text{PL}}{\text{PL}} = -\frac{\epsilon}{2(1+\epsilon)} \leq -\frac{1}{2}, \quad (S11)$$

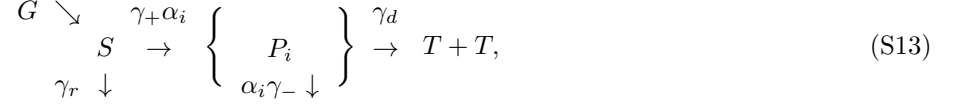
setting a maximum $\Delta\text{PL}/\text{PL}$ of 50 %, in the limit $\epsilon \gg 1$. From Eq. S10, the resonant linewidth (FWHM) is given by

$$\delta B = \frac{2V}{mg\mu_B} \sqrt{2(\epsilon+2)}, \quad (S12)$$

which grows as $\sqrt{\epsilon}$ for $\epsilon \gg 1$.

B. Triplet-Pair Emission

If instead we consider triplet pairs emitting directly, the kinetic scheme is



and $PL = \gamma_- \sum_i \alpha_i P_i$. Repeating the above procedure gives

$$PL = G\epsilon \sum_i \frac{\alpha_i^2}{(1 + \epsilon\alpha_i)} \quad (S14)$$

and

$$\frac{\Delta PL}{PL} = -\frac{1}{(\epsilon + 2)} \frac{1}{1 + \left(\frac{\Delta}{V} \sqrt{\frac{(\epsilon+1)}{(\epsilon+2)^2}} \right)}. \quad (S15)$$

At resonance,

$$\frac{\Delta PL}{PL} = -\frac{1}{\epsilon + 2} \leq -\frac{1}{2} \quad (S16)$$

which sets a maximum $\Delta PL/PL$ of 50 %, but now in the limit $\epsilon \ll 1$. The resonance linewidths are

$$\delta B = \frac{2V}{mg\mu_B} \sqrt{\frac{(\epsilon + 2)^2}{(\epsilon + 1)}}, \quad (S17)$$

which also increase as $\sqrt{\epsilon}$ for $\epsilon \gg 1$.

Comparing the two scenarios of singlet exciton emission and triplet-pair emission, only the former is able to reproduce the experimental observations of simultaneously having kinetically broadened linewidths and changes in photoluminescence approaching 50 %. Our results therefore indicate a scenario in which emission arises from singlet excitons, providing a way of distinguishing these competing kinetic models.

-
- [S1] Gélinas, S. *et al.* The binding energy of charge-transfer excitons localized at polymeric semiconductor heterojunctions. *J. Phys. Chem. C* **115**, 7114–7119 (2011).
 - [S2] Pedregosa, F. *et al.* Scikit-learn: Machine learning in Python. *J. Mach. Learn. Res.* **12**, 2825–2830 (2011).
 - [S3] Bayliss, S. L. *et al.* Spin signatures of exchange-coupled triplet pairs formed by singlet fission. *Phys. Rev. B* **94**, 045204 (2016).
 - [S4] Weiss, L. R. *et al.* Strongly exchange-coupled triplet pairs in an organic semiconductor. *Nat. Phys.* **13**, 176–181 (2017).
 - [S5] Bayliss, S. L. *et al.* Geminant and Nongeminate Recombination of Triplet Excitons Formed by Singlet Fission. *Phys. Rev. Lett.* **112**, 238701 (2014).
 - [S6] Bayliss, S. L. *et al.* Localization length scales of triplet excitons in singlet fission materials. *Phys. Rev. B* **92**, 115432 (2015).
 - [S7] Merrifield, R. E. Magnetic effects on triplet exciton interactions. *Pure Appl. Chem.* **27**, 481–498 (1971).